

Measurement of flow fields in the wake of upwind and downwind wind turbines in wind tunnel experiments

Jay Prakash GOIT*¹ and Takatsugu KAMEDA*²

The current study compares aerodynamic characteristics and performance of upwind and downwind wind turbines in wind tunnel experiments. The scaled model of wind turbine, named KDWT25, is designed and fabricated. Comparison of wake fields of the two configurations showed that the wind speed recovery in the wake of downwind turbine is faster than the upwind turbine for the uniform and laminar inflow conditions considered in this study. The tendency of turbulence profiles for both configurations is similar, with the maximum turbulence intensity observed around the rotor edge. Power coefficient at design tip speed ratio is 30% higher for the downwind turbine, even when operated in the same inflow conditions. It is assumed that the nacelle-induced blockage which deflects the flow toward more efficient outer region of the rotor, may be responsible for the better performance of the downwind turbine.

Keywords: Wind Tunnel Experiment, Downwind Turbine, Upwind Turbine, Wind Turbine Wake

1. Introduction

Large utility-scale wind turbines are predominantly horizontal-axis with three-bladed rotors. These horizontal-axis wind turbines have either upwind or downwind configuration; former have rotor upwind of towers, while later have rotor downwind of towers. Although upwind turbine configurations dominate current wind energy market around the world, downwind turbines have received significant attention in the recent years due to their potential advantages for increasing the rotor size and the rated power.

Current large-scale wind turbines have rated power of around 5 MW to 8 MW. This is expected to increase to 10-20 MW, with rotor diameters of 170 to 240 m in the near future ¹. The primary motivation for installing larger turbines is that they capture more energy from wind, thus reducing the levelized cost of energy (LCOE). Recent developments in offshore wind energy will contribute to the further increase in the sizes of turbines, since transportation, installation and operation of large wind turbines at offshore sites pose fewer challenges compared to the onshore sites. However, blades of large wind turbines can be as long as 100 m or more, and thus, in conventional upwind configuration they are prone to tower strikes. To overcome this issue, blades of large turbines are designed with increased stiffness. Furthermore, rotor

cone and tilt angles are increased in order to increase clearance between blade tip and tower². Increasing blade stiffness can significantly increase the cost of blade manufacturing, and large cone and tilt angles can reduce the turbine power output. Downwind configuration, on the other hand can have more flexible blades, since the axial load acting on blades will bend them away from the tower. They can also have lower cone and tilt angles, as they do not require large tower clearance. This will allow downwind turbines to operate close to optimum design condition thus allowing them to maintain their performances³.

Several other advantages of downwind turbines have been discussed in literatures. Nacelles of downwind turbines act as blockage to the incoming flow, such that wind is deflected radially outward on the rotors². Because the outer regions of turbine rotors are responsible for most of the power production, nacelle-induced blockage is believed to improve the output of downwind turbines ⁴. Another advantage of downwind turbines related to their performance in complex terrain was discussed by Yoshida ⁵. He showed that due to negative tilt angles, downwind turbines experience smaller misalignment with respect to up-hill flow, thus having advantage over upwind turbine configuration. Downwind turbines have tendency to align themselves with the incoming flow. This will reduce the yaw misalignment and can also be exploited for reducing the cost of the yaw control system ⁴.

Received: 19 May 2021

*¹ Department of Mechanical Engineering, Kindai University, Higashi-Hiroshima, Hiroshima 739-2116, Japan
Email jay.goit@hiro.kindai.ac.jp

*² Department of Mechanical Engineering, Kindai University, Higashi-Hiroshima, Hiroshima 739-2116, Japan
Email kameda@hiro.kindai.ac.jp

However, downwind configuration has one significant disadvantage, i.e., they experiences strong tower shadow effect⁶. Tower shadow is simply the wind speed deficit in the wake of the tower. The blades of downwind turbines experience reduced wind speed once per revolution, causing impulsive loading and rapid fluctuation in power⁷. The impulsive loads are the source of vibration of turbine structure at blade-passing frequency (BP), resulting in higher fatigue loading. Blades interaction with the tower wake is also the source of considerable low frequency noise emission⁸. Higher fatigue loads and noise emission are the primary factors why most utility-scale turbine manufacturers do not employ downwind configuration.

At the offshore sites however, noise emission is not an issue, since turbines can be installed far from the coast. Therefore, because of the above discussed advantages, downwind configuration is receiving considerable interest for large offshore wind turbine design. In this regard, Ichter *et al.*⁹ and Loth *et al.*¹ has proposed a morphing downwind-aligned rotor concept for extreme-scale wind turbines (≥ 10 MW). This unconventional morphing design is bio-inspired by palm trees, which have segmented trunks that are easily able to deflect downwind under extreme wind conditions.

Although several advantages and disadvantages of downwind configurations have been reported in the literatures, comparison of performance—in terms of power output—of the upwind and downwind turbines has not been reported to date. Difference between the flow fields around the two turbine configurations has also not received sufficient attention. In the current work we compare the aerodynamic characteristics and power performances of upwind and downwind wind turbines in wind tunnel experiments. This technical report is further organized as follows. Section 2 describes measurement setup, providing details about model wind turbines, wind tunnel facility and characterization of generator used. Flow fields and power outputs for upwind and downwind wind turbines are compared in Section 3. Finally, Section 4 provides summary of the work.

2. Measurement setup

This section describes the model wind turbine and wind tunnel setup used in the experiments.

2.1. Wind turbine model

The model wind turbine (KDWT25) used in the experimnts has both rotor diameter (D) and hub height of 0.25 m. The rotor of KDWT25 was optimized using BEMTurbine¹¹, an in-house open source tool. Following earlier studies, SD7003 airfoil profile was used along entire blade length¹². The design employed

lift (C_L) and drag (C_D) coefficient profiles at Reynolds number of 50,000. Chord length and twist angle—along the blade length—were initially optimized for tip speed ratios $\lambda = 5, 6$ and 7. Tip speed ratio is given by:

$$\lambda = \frac{\Omega R}{U} \quad (1)$$

where Ω is the angular velocity of the rotor, R is the rotor radius and U is inflow velocity. Since most utility-scale wind turbines have optimum λ value of 7, model wind turbine should also be optimized for similar λ value, in order to ensure that it has similar aerodynamic characteristics as utility-scale turbines. However, a small wind turbine with higher tip speed ratio will have very high rotational speed. For instance, if the model turbine used in this study is designed for $\lambda = 7$, its optimum rotational speed will become more than 2100 rpm (at wind speed of 4 m/s). Due to large contribution of friction loss from motor and other moving components, it is not practical to attain such a high rotor speed. As a consequence, such turbine will show significantly poor performance in terms of power output. Therefore, KDWT25 was designed to perform optimally at the lower tips speed ratio of $\lambda = 5$. For the details about the BEMTurbine and the design of KDWT25, readers are referred to Goit¹³.

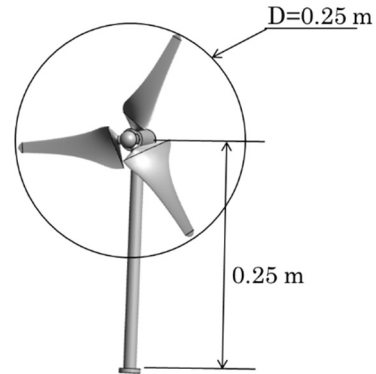


Figure 1. Design and major parameter of KDWT25

Figure 1 shows the final design of the model wind turbine. For the accurate comparison, same rotor has been used for both upwind and downwind configurations. In terms of geometrical scaling, NREL 5-MW reference wind turbine is 500 times and DTU 10-MW reference wind turbine is 700 times larger than KDWT25. The model does not have nacelle tilt or rotor pre-cone angles.

Performance of the rotor design is analyzed using blade element momentum (BEM) analysis function in the BEMTurbine. Figure 2 shows power coefficient (C_P) as a function of tip speed ratio. C_P is defined as:

$$C_P = \frac{P}{\frac{1}{2}\rho U^3 A_t} \quad (2)$$

where P is aerodynamic power of rotor, ρ is air density and $A_T = \pi/4 D^2$ is the rotor area. Maximum power coefficient of 0.47 is attained at the design tip speed ratio value of $\lambda = 5$. However, as will be clear from Section 3, $C_p = 0.47$ is very high and could not be obtained in the actual measurements.

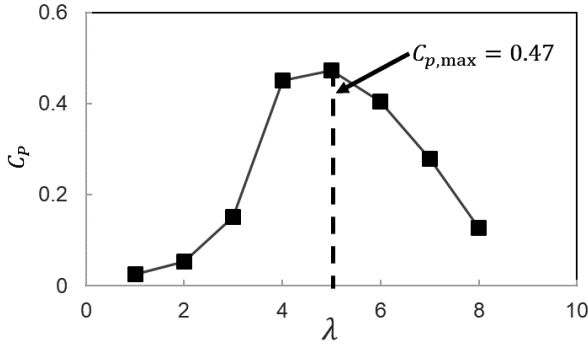


Figure 2. Power coefficient of KDWT25 as a function of tip speed ratio.

2.2 Generator performance

The generator used in the model wind turbine was brushed DC motor (Xikit XGM-RA). Usually, small DC motors are designed to perform optimally at the rotational speed of several thousand rpm. However, this DC motor can generate fairly high power at lower rpm without any gear system, thus, making it suitable for the small model wind turbine employed in this study. But there was no data available on the performance of the motor. Therefore, prior to the wind tunnel measurements, internal resistance and output characteristics of the motor was evaluated in the current study.

Figure 3 shows the schematics of the experiments for the evaluation of the motor performance. Figure 3 (a) shows the schematic of internal resistance measurement setup. In this setup, rotating disk was attached to the motor axis, and tests were conducted by supplying power at three different voltages: 5 V, 10 V and 12 V. During the measurement the disc was fixed (not allowed to rotate), so that any power loss would only be due to the internal resistance of the motor. Internal resistance (R_i) can then be computed using

$$R_i = V/I \quad (3)$$

where V and I are measured voltage and current. In order to improve the accuracy of the measurements, tests were conducted at four different disc azimuth angles: 0° , 90° , 180° and 270° for each input voltage. It was found that R_i varies between 516Ω to 550Ω . For the higher voltage though, R_i converged to 516Ω to 520Ω . Since the rotational speed of the model wind

turbine is quite high (about 1500 rpm) resulting in higher generator voltage, R_i was set to 520Ω .

Output characteristic of the motor was evaluated by coupling two motors of the same specifications as shown in Figure 3 (b). In this measurement, power was supplied at a constant voltage to motor I, and motor II was connected to a variable resistor. When both motors started to rotate, motor II would operate as a generator dumping the generated power to the resistor. Rotational speed of the system was controlled by changing the resistance value of the variable resistor, and rotational speed, current and voltage of motor II were the measurement parameters. Power output of the motors could be computed using

$$P = I^2(R + R_i) \quad (4)$$

where R is the resistance value set in the variable resistor.

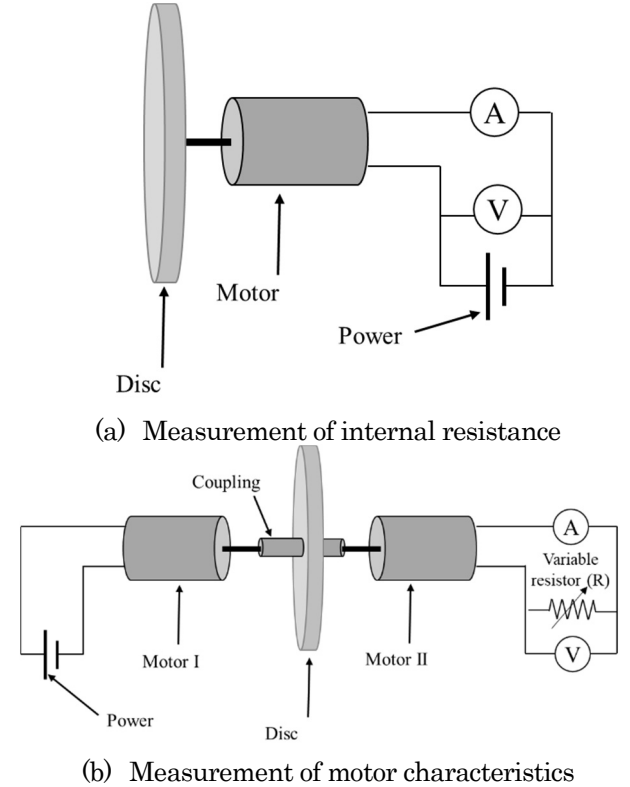


Figure 3. Schematic of motor performance evaluation tests.

Figure 4 shows the power output of motor II as a function of resistance. The measurements were conducted for four different voltages ranging from 15 V to 24 V of the motor I. The selected voltage range corresponds to the voltage range of the generator during the wind tunnel experiments. It can be appreciated that the maximum power output was generated around resistance value of 900Ω . Following this results, all wind tunnel experiments in this study were conducted by fixing the resistance-connected to the generator-to

900Ω.

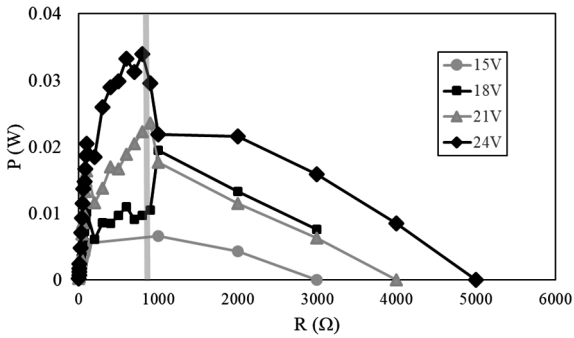
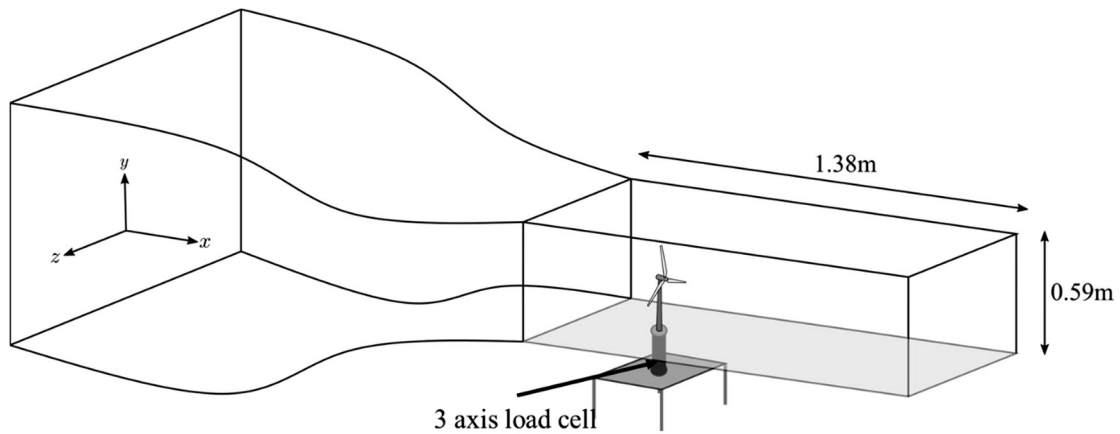


Figure 4. Motor power as a function of resistance.

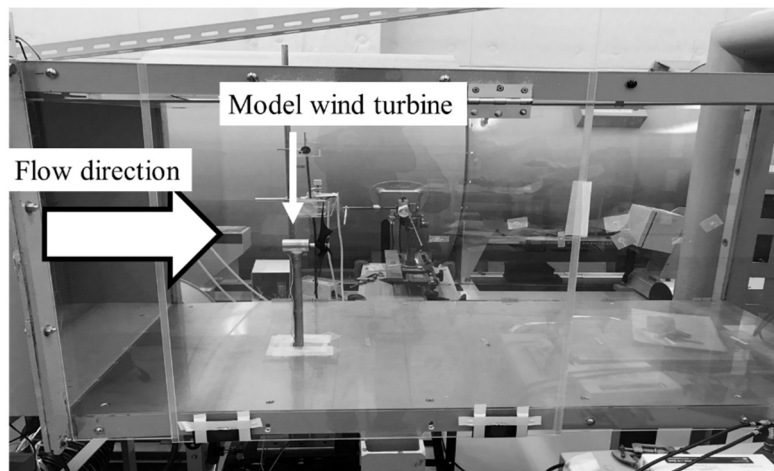
2.3 Wind tunnel

Measurements were conducted in a variable wind speed type wind tunnel at School of Engineering, Kindai University. It is a closed-circuit type wind tunnel, and has 1.38 m long test section with square cross-section of 0.59 m long sides. The blockage ratio—defined

as the rotor area to the test section cross-sectional area—is 14%. Although the blockage ratio is slightly higher than what is recommended for wind tunnel experiments, in this report we do not discuss about the effect of blockage on the accuracy of the measurements. Figure 5 shows the schematic and an actual picture of the test section with the model wind turbine installed. All the measurements were conducted at an average free stream velocity (u_0) of 4 m/s. The study used hot wire anemometry for the measurement of wind speed in the turbine wake. To that end, I-type hot wire probe (Kanomax 0248R-T5) was used. Differential manometer (Okano Seisakusho DMP-202N12) was used to calibrate the hot wire anemometer. Wind speed data was collected for the period of 10 second at 10 kHz sampling rate. Rotational speed required for the analysis of power output was measured using an external optical tachometer, while voltages and currents of the generator were measured using regular multimeters.



(a) Schematic of the wind tunnel test section



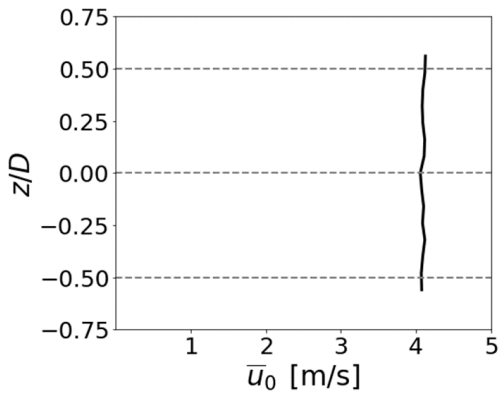
(b) Picture of model wind turbine inside the wind tunnel.

Figure 5. Wind tunnel test section.

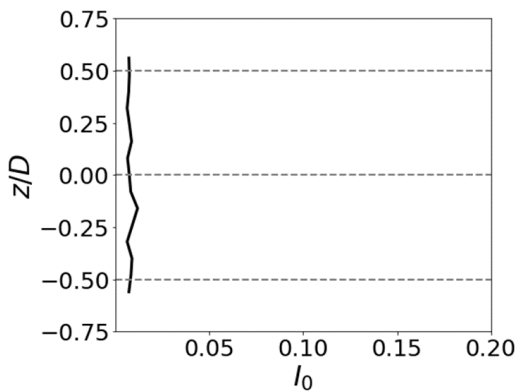
3. Results and discussion

Before the measurement and comparison of wake fields, flow characteristics of the wind tunnel was investigated. Figure 6 shows the inflow profiles of velocity and turbulence intensity before wind turbine was installed in the test section. It is appreciated that wind speed is uniform over the entire measurement span. Average velocity is 4.09 m/s which is close to the target inflow velocity of 4 m/s. Average turbulence intensity over the entire horizontal span is 0.76%. Even the highest turbulence intensity measured in this experiment is 0.84%. Therefore, it can be concluded that freestream turbulence of the wind tunnel is negligibly small.

Note that utility scale wind turbines operate in atmospheric boundary layer which is always turbulent. Turbulence intensities-at the height range corresponding to the rotor region-at offshore sites are generally around 5%, while that at onshore sites can be higher than 10%. However, for the accurate comparison of the aerodynamics characteristics of the two turbine configuration, in this study experiments were performed in uniform laminar inflow conditions.



(a) Mean velocity profile



(b) Turbulence intensity profile

Figure 6. Horizontal inflow profiles of velocity and turbulence intensity.

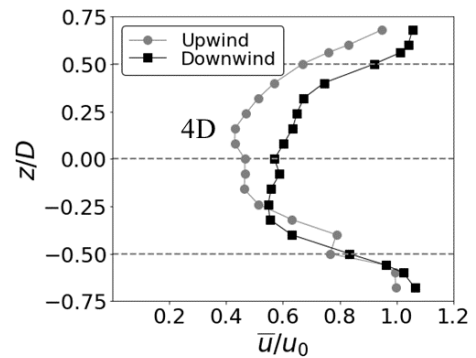
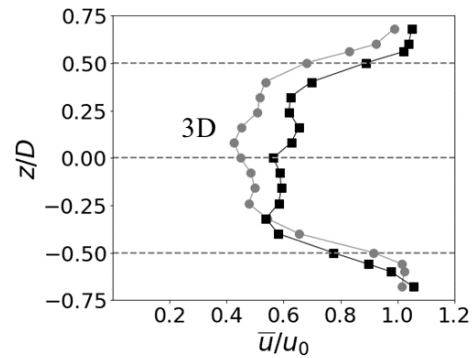
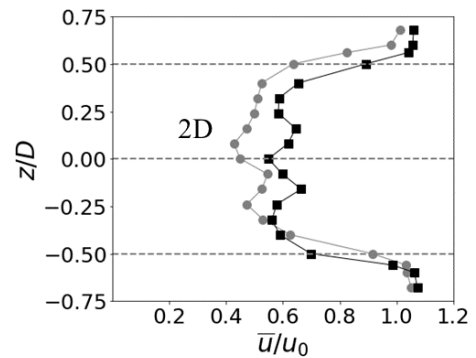
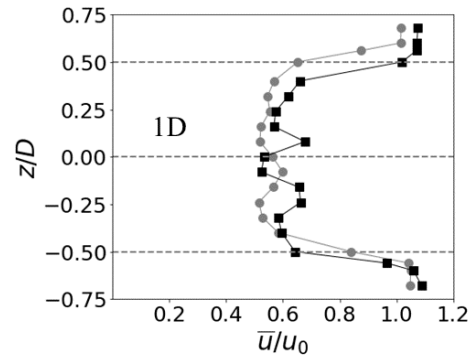


Figure 7. Comparison of horizontal mean velocity profiles at the hub height level in the wake of the upwind and downwind turbines. Dashed horizontal lines indicate position of center and edges of the rotor.

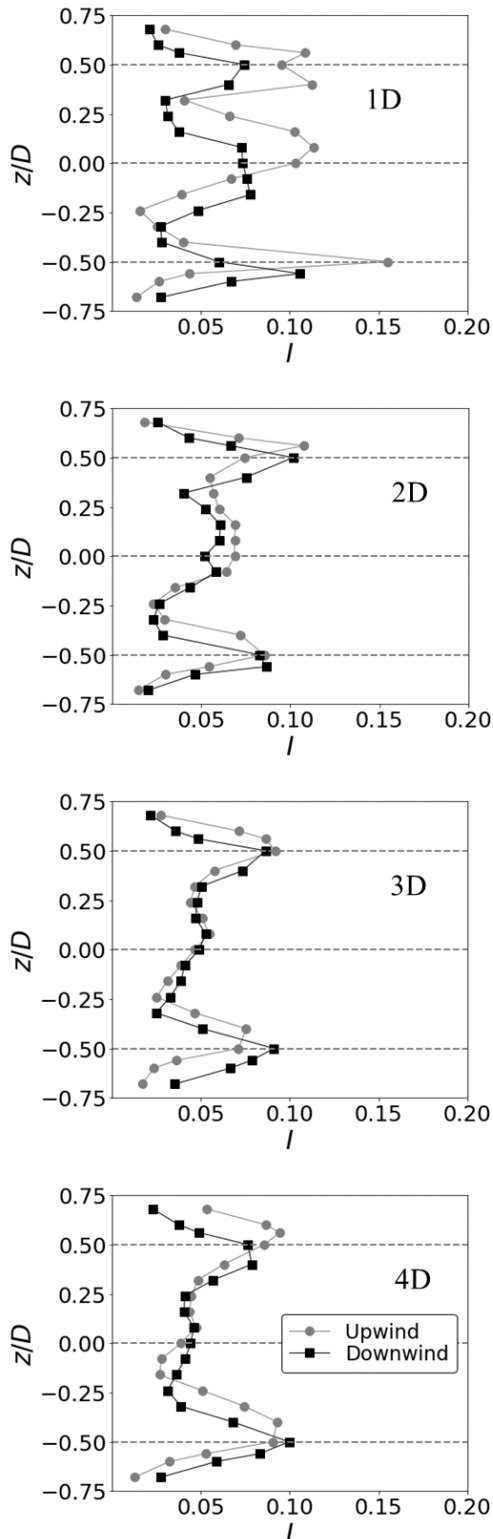


Figure 8. Comparison of horizontal turbulence intensity profiles at hub height level in the wake of the upwind and downwind turbines. Dashed-horizontal lines indicate position of center and edges of the rotor.

Figure 7 and 8 compare mean velocity and turbulence intensities in the wake of the upwind and downwind turbines. Measurements were conducted at hub height and at the spanwise interval of 20 mm. Furthermore, horizontal profiles were measured four streamwise positions, 1D, 2D, 3D, 4D downstream from the rotor. It is assumed that the difference between the wake profiles will be more conspicuous in the near-wake region considered in this study. In the far wake region, profiles of both upwind and downwind turbines should look similar.

The mean velocity profiles of both upwind and downwind configurations show similar tendencies, i.e., the largest velocity drop occurs at the center, and it gradually increases towards the edges. At 1D, velocity defects are almost same over the entire rotor region, but at downstream locations (3D and 4D) the profiles tend to have Gaussian distributions. The main difference between the wake of upwind and downwind turbines is the rate of wind speed recovery in the wake. Wake recovery is faster for the downwind turbines, resulting in the higher wind speed at 2D and further downstream positions. For example, at 4D, mean wind speed at the center of upwind turbine wake is 1.78 m/s, while that for downwind turbine wake is 2.31 m/s. This characteristic of the downwind turbine can be exploited in large wind farms. It may be possible to reduce the inter-turbine spacing if downwind turbines are used in wind farms (since their wake recovers faster). This may reduce the cost of energy from such wind farms as the required area of land lease will be smaller. However, current study only employed a single turbine. It is not possible to predict how upwind and downwind turbines will perform in a wind farm and how will they interact with the boundary layer. Detail experiments or simulations of wind farms with upwind and downwind turbines are necessary to understand the difference in the dynamics of these two configurations when installed in wind farms.

Tendency of turbulence profiles in figure 8 for both upwind and downwind configurations is also similar. Maximum turbulence intensity can be observed at the rotor edges. This is possibly due to the tip vortices resulting from the strong velocity gradient in the rotor tip region. It is observed that when turbines are placed in uniform laminar flow, added turbulence intensity due to rotor can be between 5 to 10%. In the present measurement, turbulence intensities were largest at 1D. From 2D through 4D, turbulence level in the flow did not show significant reduction. This may be due to the fact that wind turbine wakes are able to sustain its characteristics for longer downstream distance in the laminar or low turbulent ambient flow. This is the reason why the wake interaction is more significant in offshore wind farms.

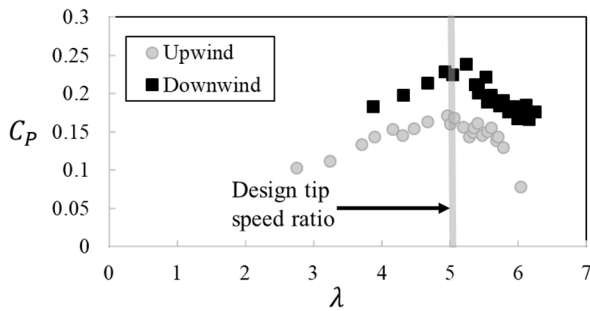


Figure 9. Comparison of power coefficients of the upwind and downwind turbines.

Finally, performance of the two turbine configuration is compared in figure 9. It shows power coefficient (C_p) as a function of tip speed ratio. It is appreciated that both turbines have the peak C_p values around the design tip speed ratio, $\lambda = 5$. The peak C_p of upwind turbine was 0.172 while that of downwind turbine was 0.24. Downwind turbine has more than 30% higher C_p compared to the upwind turbine. Better performance of downwind configuration can be attributed to its design. As also discussed in Section 1, nacelle of the downwind turbine induces blockage to the incoming flow, such that the wind is deflected towards the outer region of the rotor. Because the outer region of the rotor is responsible for most of the power production, nacelle-induced blockage may be responsible for higher efficiency of the downwind turbine.

Peak C_p in the experiments were significantly small compared to design power coefficient $C_p = 0.47$ values obtained from BEM analysis (cf. figure 2). The reason for the discrepancy lies in the fact that the rotational speeds of wind turbine in the experiments were between 800 rpm to 1800 rpm, resulting in large friction loss. Because of the higher fraction of friction loss—especially inside generators—in small model wind turbines, their C_p values obtained from measurements are generally smaller than the design C_p values.

4. Summary

In this study we have compared the aerodynamic characteristics and power performances of upwind and downwind wind turbines in wind tunnel experiments. To that end, the scaled model wind turbine, named KDWT25 was designed using an in-house open source tool BEMTurbine. Findings of the study are summarized as follows:

- (1) Wind speed recovery in the wake of downwind turbine was faster than the upwind turbine for the uniform and laminar inflow conditions considered in this study
- (2) The tendency of turbulence profiles for both upwind and downwind turbines was similar, with the maximum turbulence intensity observed at the

rotor edges. For the downstream distance from 2D through 4D, turbulence level in the flow did not show any significant reduction.

- (3) The comparison of the performance of two turbines showed that power coefficient of the downwind configuration was 30% higher than that of the upwind configuration.

Acknowledgement

The authors acknowledge Hirose International Scholarship Foundation for supporting this work. The authors would like to thank Mr. Hiroki Sunakawa and Mr. Naoyuki Kageoka of Kindai University for their assistance during the experiments. Finally, the authors are extremely grateful to Mr. Koji Umenishi of Kindai University for his help and support in the manufacturing of various components of the model wind turbines.

References

1. Loth E, Steele A, Qin C, Ichter B, Selig MS, Moriarty P. Downwind pre-aligned rotors for extreme-scale wind turbines. *Wind Energy*. 2017;20:1241–59.
2. Bortolotti P, Kapila A, Bottasso CL. Comparison between upwind and downwind designs of a 10-MW wind turbine rotor. *Wind Energy Sci*. 2019;4(1):115–25.
3. Larwood SM, Chow R. Comparison of upwind and downwind operation of the NREL Phase VI Experiment. *J Phys Conf Ser*. 2016;753(2).
4. Kress C. Downwind Wind Turbine Performance, Loading and Design Considerations. ETH; 2016.
5. Yoshida S. Performance of downwind turbines in complex terrains. *Wind Eng*. 2006;30(6):487–502.
6. Yoshida S. Combined Blade-Element Momentum—Lifting Line Model for Variable Loads on Downwind Turbine Towers. *Energies*. 2018;11:2521.
7. Manwell JF, McGowan JG, Rogers AL. Wind energy explained: theory, design and application. John Wiley&Sons Ltd, UK. 2009. 577 p.
8. Madsen HA, Johansen J, Sørensen NN, Larsen GC, Hansen MH. Simulation of low frequency noise from a downwind wind turbine rotor. In: 45th AIAA Aerospace Sciences Meeting and Exhibit. Reno, Nevada; 2007. p. 1–12.
9. Ichter B, Steele A, Loth E, Moriarty P, Selig M. A morphing downwind-aligned rotor concept based on a 13-MW wind turbine. *Wind Energy*. 2016;19:625–37.
10. Bottasso CL, Campagnolo F, Petrović V. Wind tunnel testing of scaled wind turbine models: Beyond aerodynamics. *J Wind Eng Ind Aerodyn*. 2014;127:11–28.
11. BEMTurbine Available from: <https://github.com/goitjay/BEMTurbine>

12. Schottler J, Holling A, Peinke J, Holling M. Design and implementation of a controllable model wind turbine for experimental studies. *Sci Mak Torque from Wind*. 2016;072030.
13. Goit JP. A method for the design of a scaled wind turbine for wind tunnel experiments. Vol. 11, Kindai University Fundamental Technology for Next Generation Research Institute Annual Report. 2020.